Published in final edited form as:
Microcirculation. 2008 July ; 15(5): 389–404. doi:10.1080/10739680701708436.

Arteriolar Remodeling Following Ischemic Injury Extends from Capillary to Large Arteriole in the Microcirculation

Alexander M. Bailey, **Thomas J. O'Neill IV**, **Cassandra E. Morris**, and **Shayn M. Peirce**
Department of Biomedical Engineering, University of Virginia, PO Box 800759, Charlottesville, VA 22908

Abstract

Objective—During ischemia, vascular beds in skeletal muscle have been shown to undergo arteriolar remodeling, or arteriogenesis, in order to restore tissue perfusion and function. This process has traditionally been thought to occur predominately in large vessels (diameters > 50 μm), although recent studies showing arteriogenesis in the microcirculation (diameters < 35 μm) following ultrasound-induced microbubble destruction suggest this may occur during skeletal muscle ischemia, as well. Using a surgical model of ischemia that allows *en face* visualization of microvasculature, we tested the hypothesis that ischemic injury induces arteriolar remodeling in the skeletal muscle microcirculation on the scale of capillary to sub-35 μm diameter arterioles.

Methods—Surgical ligations of the main feeding arteriole (70 μm in diameter) to the caudal-half of the spinotrapezius muscle were performed on age- and weight-matched C57BL/6 mice. The microvascular remodeling response to the ischemic insult, including enlargement and formation of new arterioles, as well as degree of vascular branching and collateral formation, were then quantified and compared to contralateral control muscles using intravital and whole-mount confocal microscopy. Immunohistochemical techniques were used to verify the presence of inflammatory cells (monocytes and tissue-resident macrophages; MOMA-2+ or CD11b+), as well as the absence of chronic hypoxia (Hypoxyprobe-1+ kit; Chemicon International).

Results—Five days post-arteriole ligation, ischemic tissue underwent reproducible and localized microvascular remodeling characteristic of arteriogenesis. Using intravital microscopy and examining functional vessels (arterioles and venules) with diameters 15–35 μm, we observed significant increases in vascular density (38%), branching (90%) and collateral development (36.5%). The formation of new arterioles (diameters 6–35 μm) was quantified and significantly increased, as evidenced by expanded smooth-muscle α-actin (24.3%) arteriolar-coverage. However, arcade arteriole (AA) length densities did not significantly increase following ligation. The absence of chronic hypoxia and pronounced vessel tortuosity was also consistently observed.

Conclusions—Ischemic ligations induce arteriolar remodeling responses in the microcirculation (vessel diameters < 35 μm) of the spinotrapezius muscle in the C57BL/6 mouse. Furthermore, the surgical model that allowed this quantification enabled *en face* analysis of skeletal muscle microvascular network adaptations with single-cell resolution and has the capability to provide investigators with functional and morphometric data on a microscale difficult to achieve using other animal models.

Corresponding Author: Alexander M. Bailey, Department of Biomedical Engineering, University of Virginia, PO Box 800759, Charlottesville, VA 22908, Phone: 434-243-9892, Fax: 434-982-3870, amb3gq@virginia.edu.

Keywords

spinotrapezius; hindlimb; animal model; ischemia; arteriogenesis; arterialization; collateral; vascular remodeling; microcirculation; microvessel; hypoxia; arteriole; monocyte; arcade; transverse

Introduction

During ischemia, blood supply to a tissue is deleteriously decreased by the constriction or obstruction of the upstream vasculature. In an attempt to restore perfusion to the injured tissue, the body's natural response is to undergo arteriolar remodeling, or arteriogenesis [1, 2]. Although this process has traditionally been thought to occur primarily in larger vessels (Table 1), limitations in existing animal models and experimental techniques have prevented rigorous investigation at the microscale level within the microcirculatory system, defined here as vessel diameters < 35 μm.

The current *in vivo* standard for the study of ischemia-induced arteriolar remodeling is the hindlimb ischemia model, most often performed in the gracilis muscle of rabbits, rats, or mice by ligating either the common iliac artery, femoral artery, and/or some combination of their superficial branches [3–6]. These models of ischemia, or slight variations thereof, have been used extensively to study vascular remodeling in the presence of exogenous growth factor delivery [4], therapeutic stem cell delivery [6], inflammation [7], and during diabetes [8]. The hindlimb models are highly relevant for the study of ischemia, particularly investigation of treatment methods for peripheral vascular disease, in that they effect downstream muscles to varying degrees (as a function of location, vascular architecture, and metabolic demand) thus allowing study of distant and local ischemic tissue beds [9], are amenable to laser-Doppler perfusion imaging (LDPI) to quantify degrees of tissue perfusion [7], and allow visualization of gross tissue-level changes (e.g., development of necrotic foot and auto-amputation [6]).

Another model of skeletal muscle ischemia, the rat spinotrapezius model, has been used to study muscle fiber contractility [10], as well as inflammation and leukocyte adhesion [11, 12]. Following the ligation or obstruction of feeder arterioles, the spinotrapezius muscle can be exposed and observed *in situ* for investigation of network-level vascular properties, and it can also be undermined and exteriorized for more detailed investigation [13], such as RBC and microbubble trafficking through microvessels < 7 μm, for example [14]. Resolution can be further enhanced through the use of young rats with thinner muscles. This stabilizing, skeletal muscle is well perfused with natural arcade arteriole loops and collateral vessels [15–18], similar to the human heart (despite much steeper metabolic demands and greater function) and so may be particularly relevant to the study of ischemic cardiac pathologies. However, it is also a superficial muscle unable to be exercised in isolation, and so the physiological and pathological responses to ischemia observed here may not be conserved in other muscular tissues.

Both the mouse hindlimb and rat spinotrapezius ischemia models have been used to investigate complex phenomena. They can be combined with western blotting, confocal immunofluorescence, gene and protein arrays, blood flow measurements (e.g., LDPI), intravital microscopy, and/or biochemical assays (e.g., ELISAS) which further expands the scope of questions able to be addressed, as well as facilitates investigation of pathologies while considering both spatial and temporal influences. Furthermore, paired contralateral muscles are able to act as internal controls and allow for the investigation of any systemic effects.

These models have contributed greatly to the understanding of ischemia-induced arteriogenesis, although limitations have made it difficult to investigate arteriolar remodeling events in microvessels with diameters < 35 μm. In the hindlimb model, the thickness of the gracilis and abductor muscles often requires tissues to be sectioned for visualization and analysis of the microvasculature, thus preventing assessment of intact vascular networks. To retain spatial relationships, angiography and microCT techniques are often employed, although resolution is inadequate (lower limit of 35 μm diameter vessels using microangiography [19–21] and 25 μm using microCT [22]), and visualization and quantification of microvessels is difficult [23]. Conversely, intravital and more detailed whole-mount microscopy in the rat spinotrapezius is possible. However, resolution of microvessels across the entire muscle is often poor, and visualization of intact microvessels with single-cell resolution is extremely difficult, even with the addition of partial tissue digestions following harvest from young rats.

The processes of arteriogenesis, or the growth and formation of collateral vessels, in large arterioles (diameters > 35 μm) during skeletal muscle ischemia is indisputable. These phenomena are primarily responsible for the restoration of tissue perfusion, although, theoretically, local microvessels (diameters < 35 μm) could aid as well. Recent studies investigating arteriogenesis following ultrasound-induced microbubble destruction have shown that remodeling can occur at the microvessel level [24], and changes here can have significant effects on reductions in network resistance [25–27]. The microvessel contribution on network flow resistance reduction during skeletal muscle ischemia, however, remains largely unknown (Table 1). Difficulties in the ability of current ischemia models to perform a detailed analysis simultaneously at the cellular and tissue-level scale have partly contributed to this gap in knowledge.

To investigate arteriolar remodeling in the microcirculatory system, we have developed a mouse model of skeletal muscle ischemia. A natural and logical extension of other *in vivo* models of ischemia, this model uniquely allowed investigation of arteriolar remodeling in intact microvessels across entire skeletal muscles, without having to surgically exteriorize the muscle. Specifically, we use an arteriole ligation strategy to create ischemic injuries that induce localized and reproducible vascular remodeling responses in the spinotrapezius muscle (Figure 1). This pair of skeletal muscles, located on the dorsum adjacent to either side of the spine and running between the 4^{th} thoracic and 3^{rd} lumbar vertebrate, are stabilizing muscles that contain intrinsic microvascular beds. It inserts in the spine and scapula and is well innervated with the majority of nerves running within 200 μm of arterioles [28]. Like the rat spinotrapezius muscle, it is well perfused with highly developed collateral vessels and arcade arteriole loops, but unlike the rat, it is thin throughout the extent of its length and width (60–200 μm thick), thus allowing *en face* visualization of the muscle tissue and microvascular networks contained therein using both intravital and whole-mount confocal microscopy [29]. By utilizing this approach, we preserved vascular spatial relationships and were thus able to distinguish between arcade arterioles (AA) and transverse arterioles (TA). This may be important for furthering our understanding of arteriogenesis, which is thought to occur predominately in AA, or anastomoses, and not in TA.

Materials and Methods

Mouse study groups

Sixteen male C57BL/6 mice (Harlan, Indianapolis, IN), age-matched and weighing between 27 and 32 g were grouped according to the procedures they received: ischemic ligation, sham control, or none (“day 0” with no intervention). Each mouse received either an ischemic ligation or a sham surgery in their left spinotrapezius muscle and no treatment in

their right contralateral control muscle. The experimental groups and respective treatments in the left and right muscles are abbreviated as indicated below:

Group I Day 0 (Left, Right): φL, φR

Group II Sham Control (Left, Right): SL, SR

Group III Ischemic (Left, Right): IL, IR

Surgical Intervention

The following animal procedures were approved by the Animal Care and Use Committee of the University of Virginia. Mice were anesthetized (intraperitoneal (i.p.) injection of ketamine/xylazine/atropine; 60/4/0.2 mg/kg) and a horse-shoe shaped incision (~3–5 mm) was made through the dorsal skin approximately 5 mm caudal to the bony prominence of the shoulder blade. Under a dissecting microscope, blunt dissection was used to separate, but not remove, the white-fat pad from the underlying muscular tissue in order to visualize the vasculature. The main feeding arteriole (visibly the largest) to the caudal-half of the muscle was then located and visually followed upstream (cranially) until it crossed the lateral border and exited the spinotrapezius. Being careful to minimize any mechanical wounding (no additional incisions), blunt dissection was used to isolate the arteriole from its associated venule. Using 10-0 suture, a ligature was placed around this arteriole (~0.07 mm in diameter). Successful ligations were verified by visually observing a complete diminution of arteriole blood flow (obstructed RBC column) downstream from the ligature. The incision was then closed with 7-0 non-resorbable sutures, and the animal was allowed to recover. Warmed Ringers solution (37°C) with adenosine (0.14g/0.5L), a potent vasodilator, was superfused onto the tissue throughout the surgery to aid in the visualization of vessel architecture. Of note, a second artery-vein pair runs closely along the spine, eventually branching into the re-positioned fat pad, and care was taken to avoid disrupting these vessels. During the sham surgeries, the main feeding arteriole was separated from its associated venule in the same fashion; only the ligature placement was simulated (suture was passed around the arteriole, but not knotted nor left in the animal). Adenosine was applied during the sham surgeries.

Intravital microscopy and image analysis

Mice were anesthetized and intravital microscopy was used to visualize perfused (functional) vessels in the spinotrapezius muscles prior to harvesting. Entire spinotrapezius muscles were exposed, but not exteriorized, by retracting the overlying skin and fascia. A 37°C mixture of Ringer's Solution with adenosine (0.14g/0.5L) was superfused onto the exposed area for 20 minutes to abolish any inherent vascular tone (maximally dilate). No mechanical manipulation of the muscle tissue was performed. Specimens were imaged at 6.25x using a Makroskop M420 (5x-32x) and an Olympus Microfire color digital camera. To ensure accurate measurements and accommodate the varying topography of the dorsum, multiple pictures of each specimen were taken at differing focal planes.

Analysis and contrast enhancement of intravital microscopy images were conducted using the ImageJ (National Institutes of Health, Bethesda MD) imaging software suite. This allowed analysis of perfused (functional) microvessels as small as 15μm in diameter (resolution limit as identified by visualizing the red blood cell columns in each vessel). Total functional vessel lengths per unit area (vascular densities) were quantified in the "ischemic zone." This zone included the majority of the caudal-half of the spinotrapezius muscle and was defined as the trapezoidal area bounded by 4 lines: *Line #1*) a line nearly parallel to the spine drawn from the first vessel branch point downstream of the ligation site to the feeding artery at the caudal end of the spinotrapezius muscle, *Line #2*) a line drawn parallel to the spine and 1 mm lateral to the spine, *Line #3*) a perpendicular line extending from line #1

(intersecting it at the first vessel branch point downstream of the ligation site) to line #2, and *Line #4*) a perpendicular line extending from line #1 (intersecting it at the caudal end of the muscle) to line #2. Demarcations of this zone are shown in Figure 2A. The numbers of vascular branches originating from the spinal vessels adjacent to either spinotrapezius muscle were quantified, as well as the numbers of vessels that crossed within 1 mm of the spine (termed "bridging collaterals"), regardless of their origin. The arteriole inputs to the ischemic zone were consistently observed to be ~30–40 μm in diameter. It is reasonable to assume, therefore, that the ischemic zone consists of a network of smaller-sized vessel branches and loops.

Spinotrapezius Tissue Harvest

Anesthetized mice were euthanized with sodium pentobarbital (i.p. overdose injection), and circulating cells were removed from the vasculature with an intracardial infusion of 0.9% heparanized saline. Spinotrapezius muscles were then excised and fixed on gelatin-coated glass slides by immersion in chilled methanol (4°C) or in a 4% parafomaldehyde/de-ionized water solution at room temperature for 20 min. Immediately following fixation, specimens were washed four times for 20 minutes each using 0.01M phosphate-buffered saline (PBS) with 0.1% saponin (Sigma).

Whole-mount Immunohistochemistry

Spinotrapezius tissues were immunolabeled for lectin, smooth-muscle α-actin (αSMA), desmin, CD11b, CD45, MOMA-2, and/or NG2 proteoglycan using the following protocol. Following the post-fixation washes, tissues were incubated with primary antibody solutions for 20 hours at room temperature (RT). Following primary incubation, tissues were again washed four times for 20 min each using PBS with 0.1% saponin before incubation with secondary antibody solutions for 20 hours at RT. Antibodies were diluted in buffer consisting of PBS, 0.1% saponin, 2% bovine serum albumin, and either 5% normal donkey or normal goat serum, as described below.

Dilutions were tailored to the specific antibody used. Briefly, endothelial cells were identified using isolectin GS-IB_4 conjugated to Alexa-568 (Molecular Probes; 1:200 dilution). Smooth muscle and perivascular cells were identified with Cy-3-conjugated monoclonal anti-smooth muscle α-actin (αSMA) clone 1A4 (Sigma; 1:150 dilution), rabbit anti-NG2 chondroitin sulfate proteoglycan polyclonal (Chemicon International; 1:100 dilution) with Cy2-conjugated IgG secondary (Jackson ImmunoResearch, 1:200 dilution), and goat anti-desmin (C-18) polyclonal (Santa Cruz Biotechnology, Inc.; 1:100 dilution) with Cy2 conjugated donkey-anti-goat secondary (Jackson ImmunoResearch; 1:200 dilution). Tissue-resident inflammatory cells were identified using either biotinylated CD11b rat monoclonal (Serotec; clone M1/70.15; 1:200 dilution) with Streptavidin-conjugated Alexa488 secondary antibodies (Molecular Probes; 1:200 dilution), or rat-anti-mouse macrophages/monocytes monoclonal antibody (Serotec; clone MOMA-2; 1:100 dilution) with goat-anti-rat Cy3 secondary antibodies (Jackson ImmunoResearch; 1:200 dilution). MOMA-2 recognizes an intracellular antigen of mouse macrophages and monocytes.

Digital images of immuno-labeled whole-mount spinotrapezius tissue were acquired using confocal microscopy (Nikon, Model TE200-E2; 4x, 10x, 20x, and 60x objectives). Analysis of the confocal images was conducted using ImageJ imaging software to quantify the number of αSMA-positive arterioles within the ischemic zone. An arteriole phenotype was denoted by intense αSMA staining and tight perivascular cell wrapping. Using this antibody allowed visualization and quantification of microvessels as small as 6 μm in diameter.

Tissue Hypoxia Measurements

Regions of hypoxia (pO_2<10 mm Hg) were identified using a primary FITC-conjugated mouse monoclonal antibody directed against pimonidazole protein adducts, along with a secondary mouse anti-FITC horseradish peroxidase (HRP) antibody (Hypoxyprobe-1+ kit; Chemicon International). Briefly, surgical ligations to induce ischemic injury were placed around feeder arterioles in spinotrapezius muscles of C57BL/6 mice, and i.p. injections of pimonidazole hydrochloride (1ml vol. at 60mg/kg) were given 48 hours post-ligation. Twenty minutes after i.p. injection, anesthetized mice were euthanized and the spinotrapezius muscles and liver were excised, fixed in 4% parafomaldehyde/de-ionized water for 48 hours, paraffin-embedded, and sectioned sagitally (5 μm thick sections). Immunohistochemical analysis was preformed to identify regions of hypoxia. Tissues were incubated with the primary reagent (1:50 dilution) for 30 minutes at RT, followed by the secondary reagent (1:50 dilution) for 30 minutes at RT during standard Hematoxylin and Eosin (H&E) counter-staining procedures. Liver is naturally at or below a pO_2 of 10mm Hg, and therefore serves as an internal positive control for this staining procedure.

Statistical Analysis

All statistical comparisons were made using the statistical analysis tools provided by SigmaStat 5.0 (Systat, Inc., Point Richmond, CA). Results are presented in the form of mean ± standard deviation (SD). Data in Figures 3, 4A, and Table 2 were tested for normality and then analyzed by one-way ANOVA followed by non-paired Tukey's T-test. Data in Figure 4B were analyzed using paired T-test. In all cases, statistical significance was asserted at $p \leq 0.05$.

Results

Microvascular architectures

The caudal-half of the spinotrapezius tissue in the C57BL/6 mouse is well perfused. A simplified cartoon representation of three main feeder arterioles is shown in Figure 1A. Ligations were placed around one of these main feeding arterioles (location depicted in Figure 1B at the "X," upstream of white arrow in Figure 2A, and upstream of the black arrow in Figure 5A), and collaterogenesis consistently occurred in at least one of three general areas (Figure 1B; numbers). These collateral vessels adopted a tortuous phenotype, characteristic of collateral vessel formation during arteriogenesis.

En face visualization and quantification of microvessels after ischemic ligation

Intravital microscopy allowed the visualization of perfused vessels (arterioles and venules) with diameters larger than 15 μm. Both spinotrapezius muscles were observed lateral to the spine (indicated by dashed lines), with feeding arterioles and draining venules clearly evident in a macroscopic view of the exposed mouse dorsum on day 0 (Figure 2A). The approximate location of the caudal-half of the spinotrapezius, termed the "ischemic zone," can be seen bounded by the four solid lines forming the white trapezoid. Vasculature that branched off of the spinal vessels and perfused the spinotrapezius tissues was also apparent, shown here in a mouse that received ischemic ligations five days prior (Figure 2B). Following ischemic ligation, structural changes were observed using intravital microscopy, including pronounced vessel tortuosity (white arrows) and branching (Figure 2B–C), which was not seen in the paired unligated muscle.

The vascular density of perfused vessels (arterioles and venules) with diameters greater than 15 μm in the ischemic zone increased 37.7% over that in the contralateral control side (Figure 3). In comparison, sham ligation induced a negligible (1%) decrease in this metric compared to the respective contralateral side. Within the control study group (day 0),

functional vessel density was consistently identical in left and right muscles (percent change equal to zero).

The ischemic intervention also increased the amount of perfused vessel branches and bridging collaterals, as observed using intravital microscopy. Following ligation, there were increased numbers of vessels 15 μm in diameter or greater branching off of the spinal vessels in the direction of the ischemic zone when compared to the sham and day 0 tissues (Figure 4A). Conversely, there were no significant changes in the amount of vascular branches observed in the contralateral control tissues. Bridging collaterals were defined as any vessel (arteriole or venule) that crossed within 1 mm of the spinal vessels from any direction, independent of origin. Five days post-ligation, there was a significant increase in the amount of observed bridging collateral vessels in ischemic tissue when compared to their paired contralateral controls (Figure 4B). There were no observed differences in this metric in tissues receiving sham surgeries, or in the left and right muscles on day 0 prior to any treatment. This location where collaterogenesis was quantified is depicted in Figure 1 (zone 1). The other two zones where collaterogenesis was often observed were not quantified.

Ischemic ligation produces reproducible zones of arteriolar remodeling

In the ischemic muscle, immunohistochemical analysis revealed that the total length of microvessels (arterioles only; diameters > 6 μm) containing αSMA-positive perivascular cells was increased relative to the contralateral control muscle (Figure 5: Compare A with B). This increased length was repeatedly observed predominately in the caudal-half (ischemic zone) of the spinotrapezius muscle (Figure 5A: compare top half to bottom half). Similar observations were made in three other pairs of muscles. The apparent size discrepancy between muscles is due to variations in the harvesting procedure and not physiological or pathological changes in tissue properties.

The coverage of arterioles with αSMA-positive perivascular cells (length per unit area) in the ischemic zones was quantified and found to be elevated by 24% over that in the corresponding zone of the contralateral control muscles (Table 2). Conversely, the length densities of αSMA+ arcade arterioles (AA) in the ischemic zone were not significantly increased, nor were the number of arcade loops, when compared to contralateral controls (Table 2).

Inflammatory cell presence

Twenty-four hours post ligation, spinotrapezius muscles were harvested and immunolabeled for CD11b and MOMA-2 antibodies. Inflammatory cells positive for CD11b were detected in tissues receiving sham (Figure 6A) or ischemic ligations (Figure 6B), as well as in respective contralateral controls (images not shown). MOMA-2 positive inflammatory cells were detected in tissues receiving ischemic ligations (Figure 6C). In spinotrapezius muscles of control mice that received no intervention (day 0), little to no instances of positive CD11b or MOMA-2 were detected (data not shown). Circulating and tissue-resident inflammatory cells that immunolabel for MOMA-2 and/or CD11b have been shown to mediate arteriogenic responses in other similar models of skeletal muscle ischemia (Table 1).

Ischemic ligation does not induce chronic hypoxia

Spinotrapezius muscles and liver were harvested 48 hours post-ligation or post-sham surgery and probed for the presence of hypoxic gradients using the Hypoxyprobe-1+ kit from Chemicon International. Tissues were developed using 3,3′-diamnobenzidine (DAB), and the presence of brown cells indicated cell exposure to oxygen tensions of less than 10 mm Hg (oxygen concentration of 14 micromolar). Neither ischemic nor sham tissues contained detectable amounts of hypoxic cells (Figures 6D and 6E), nor did any contralateral control

tissues (images not shown). Liver served as the positive control to verify that the Hypoxyprobe-1 compound was active, and, as expected, liver tissue stained positive for low oxygen tensions (Figure 6F).

Whole-mount immunohistochemistry with single-cell resolution

Whole-mount immunohistochemistry and confocal microscopy allowed visualization of single cells and tissue-level views of microvascular architecture while preserving spatial relationships. Specifically, vascular smooth muscle cells in arterioles (Figure 7A and 7B) and venules (Figure 7A and 7C), as well as perivascular cells throughout the vasculature were observed (Figure 8). Note that cellular processes were identifiable (Figure 8C and 8D, white arrows) and that close cell apposition/wrapping morphology exhibited by perivascular cells along endothelial cells was visible.

Discussion

The participation of microvessels during ischemia-induced arteriogenesis in skeletal muscle on the scale of capillary to sub-35 μm diameter arterioles has not been rigorously investigated. We show here that ischemic ligations of the main feeder arteriole to the caudal-half of the spinotrapezius muscle in the C57BL/6 mouse induced reproducible and localized arteriolar and microvascular changes on this scale. Specifically, we quantified five-days after arteriole ligation an enlargement and expansion of perfused (functional) vessels as manifested through increased vessel density, collateral formation, and branching of vessels 15–35 μm in diameter. Pronounced vessel tortuosity was also observed, and the formation and/or enlargement of new arterioles was quantified and significantly elevated, as evidenced by expanded αSMA coverage on arteriolar-networks (arterioles with diameters > 6 μm). Chronic hypoxia was ruled out as a dominant stimulus, and the mobilization of inflammatory cells to the ischemic tissue was documented.

Microvascular remodeling changes within the ischemic skeletal muscle's capillary bed, however, were not investigated. Largely because of the limitations of intravital microscopy, we were unable to examine vasculature less than 15 μm in diameter. It is therefore unclear whether angiogenesis, increased branching, or smaller collateral formation is also occurring. Rather, the increased observation of these events in vasculature greater than 15 μm in diameter is indicative of an active vessel enlargement phenomena.

The definition employed in this study for the quantification of arteriogenesis is consistent with that used in the study of arteriolar remodeling in larger vessels in existing animal injury models (Table 1). Specifically, arterioles were identified by their morphology and positive-αSMA coverage, and tissue-resident macrophages were identified by positive immunolabeling for MOMA-2. Furthermore, the development of tortuous collateral vessels and the vessel enlargement that we observed is similar to that seen in other animal models (Table 1) and during the pathological response to heart disease [30–32] (e.g., coronary artery stenosis). However, unlike many other models, spatial detail at the microvascular level was preserved. Tissue sectioning can make it difficult to distinguish between arcade and transverse arterioles, but we were able to easily make that distinction here, at the microscale level. In this way, it was possible to impeccably determine whether a αSMA-positive vessel segment was part of a collateral vessel. This may be important for the future study of ischemia-induced arteriogenesis in the microcirculation because, while it has been shown to be constrained to pre-existing AA, their relative contribution (versus TA for example) cannot always be easily quantified (Table 1).

Even though ischemia-induced arteriogenesis in the skeletal muscle microcirculation has not been previously observed (Table 1), arteriolar remodeling on this scale is not without

precedent. Price et al. observed enlargement and remodeling of 9–27 μm diameter arterioles following ultrasound-inducted microbubble destruction [24], and Silvestrie et al. showed 2-fold increases in micro-arteriole density in interleukin-10 transfected mice [33]. In a model of ischemia in rat mesentery (thin connective tissue), Van Gieson et. al. documented enhanced coverage of < 40 μm diameter vessels with mature smooth-muscle cells (MHC+) in response to elevated pressure and wall strain [34]. We complement these studies by showing here that significant sub-35 μm diameter arteriolar and microvascular remodeling can occur in response to ischemic ligation in skeletal muscle, as well.

The exact mechanisms governing this remodeling response have not been explicitly shown and are still unclear. However, the lack of chronic hypoxia in the ischemic tissue, as well as the low observed incidence of microvascular remodeling following sham ligation suggests that the primary stimuli are the changing blood flow profiles and hemodynamic force alterations following ligation. If proved to be true, this would be consistent with the current understanding of arteriogenesis [35]. Currently, obtaining accurate *in vivo* measurements of blood flow velocities and pressure distributions within the microvasculature is difficult and so were not conducted in this study, although this should be addressed in future studies. Additionally, the effects of transient low oxygen tension cannot be discounted. Immediately following surgery, it is possible that acute hypoxia downstream of the ligation was induced, and so it could be a contributing stimulus to the observed microvascular remodeling.

It is also unclear whether similar remodeling responses may be occurring following induction of ischemia in the hindlimb models. Because other models often requite tissue sectioning to visualize the microvasculature, the loss of spatial detail (and lack of absolute vessel counts) may make it difficult to observe modest changes at this scale if they are indeed occurring. This could explain why the phenomena we describe here has gone unreported in other injury models. Moreover, the reported arteriogenesis in skeletal muscle vasculature may be unique to the spinotrapezius muscle and/or the specific surgical methods. The spinotrapezius and hindlimb (gracilis and abductor) muscles are anatomically different; the former naturally contains many more arcade arteriole loops, although both possess similar capillary to muscle fiber ratios and undergo microvascular remodeling following exercise regimens [18]. It is also possible that the diameter of the ligated or obstructed vessel is critical in determining the specific remodeling response (femoral and iliac arteries are much larger than the vessel ligated in this model). As such, a blockage in blood flow in larger vessels would likely result in the re-routing of blood through similarly sized collateral vessels, thus inducing many of the arteriogenic stimuli locally as opposed to in downstream sub-35 μm arterioles. Regardless, such investigation is still of relevance as it could lead to a more complete understanding of the mechanisms of arteriogenesis and also new treatment strategies to induce arteriolar remodeling on a wider scale. For example, following myocardial infarction, it may be possible to promote a therapeutically-enhanced arteriogenic response that extends from capillary (6 μm diameter), shown here, to large arteriole (200 μm+ diameter) levels, shown previously.

To facilitate the study of arteriogenesis in the microvasculature (vessel diameters < 35 μm) of skeletal muscle during ischemia, we extended and adapted existing surgical models to the mouse spinotrapezius muscle. Here, we were able to study vascular changes with single-cell resolution and observe networks *en face*, thus preserving both cellular- and tissue-level properties. It also facilitated the simultaneous use of qualitative and quantitative assessment tools including: 1) intravital microscopy that can provide a measurement of functional length density while preserving spatial detail and muscle integrity (e.g., no exteriorization is needed), 2) whole-mount immunohistochemistry that allows spatial analysis of intact vascular networks, and 3) confocal microscopy that enables 3-D visualization of cell morphometry. Moreover, it lends itself to use in an array of transgenic studies, where

molecular mechanisms may be explored in more detail. The development of models such as this is critical for acquiring a better understanding of the physiological response to ischemia, so that improved therapies, for heart disease and peripheral vascular disease in particular, may be designed and tested. To conclude, we report that the microvasculature (diameters < 35 μm) following ischemic ligation of the spinotrapezius muscle in the C57BL/6 mouse undergoes significant arteriolar and microvascular remodeling.

Acknowledgments

Funded by the University of Virginia Department of Biomedical Engineering

References

1. Peirce SM, Skalak TC. Microvascular remodeling: a complex continuum spanning angiogenesis to arteriogenesis. Microcirculation. 2003; 10(1):99–111. [PubMed: 12610666]
2. Heil M, et al. Arteriogenesis versus angiogenesis: similarities and differences. J Cell Mol Med. 2006; 10(1):45–55. [PubMed: 16563221]
3. Hershey JC, et al. Revascularization in the rabbit hindlimb: dissociation between capillary sprouting and arteriogenesis. Cardiovasc Res. 2001; 49(3):618–25. [PubMed: 11166275]
4. Leong-Poi H, et al. Assessment of endogenous and therapeutic arteriogenesis by contrast ultrasound molecular imaging of integrin expression. Circulation. 2005; 111(24):3248–54. [PubMed: 15956135]
5. Miranville A, et al. Improvement of postnatal neovascularization by human adipose tissue-derived stem cells. Circulation. 2004; 110(3):349–55. [PubMed: 15238461]
6. Rehman J, et al. Secretion of angiogenic and antiapoptotic factors by human adipose stromal cells. Circulation. 2004; 109(10):1292–8. [PubMed: 14993122]
7. Egami K, et al. Ischemia-induced angiogenesis: role of inflammatory response mediated by P-selectin. J Leukoc Biol. 2006; 79(5):971–6. [PubMed: 16641139]
8. Schiekofer S, et al. Impaired revascularization in a mouse model of type 2 diabetes is associated with dysregulation of a complex angiogenic-regulatory network. Arterioscler Thromb Vasc Biol. 2005; 25(8):1603–9. [PubMed: 15920034]
9. Arras M, et al. Monocyte activation in angiogenesis and collateral growth in the rabbit hindlimb. J Clin Invest. 1998; 101(1):40–50. [PubMed: 9421464]
10. Suzuki H, et al. Temporal correlation between maximum tetanic force and cell death in postischemic rat skeletal muscle. J Clin Invest. 1995; 96(6):2892–7. [PubMed: 8675660]
11. Harris AG, Skalak TC. Effects of leukocyte capillary plugging in skeletal muscle ischemia-reperfusion injury. Am J Physiol. 1996; 271(6 Pt 2):H2653–60. [PubMed: 8997328]
12. Kadambi A, Skalak TC. Role of leukocytes and tissue-derived oxidants in short-term skeletal muscle ischemia-reperfusion injury. Am J Physiol Heart Circ Physiol. 2000; 278(2):H435–43. [PubMed: 10666073]
13. Bailey JK, et al. Spinotrapezius muscle microcirculatory function: effects of surgical exteriorization. Am J Physiol Heart Circ Physiol. 2000; 279(6):H3131–7. [PubMed: 11087272]
14. Price RJ, et al. Delivery of colloidal particles and red blood cells to tissue through microvessel ruptures created by targeted microbubble destruction with ultrasound. Circulation. 1998; 98(13): 1264–7. [PubMed: 9751673]
15. Engelson ET, Schmid-Schonbein GW, Zweifach BW. The microvasculature in skeletal muscle. II. Arteriolar network anatomy in normotensive and spontaneously hypertensive rats. Microvasc Res. 1986; 31(3):356–74. [PubMed: 3713551]
16. Kindig CA, Poole DC. A comparison of the microcirculation in the rat spinotrapezius and diaphragm muscles. Microvasc Res. 1998; 55(3):249–59. [PubMed: 9657925]
17. Skalak TC, Schmid-Schonbein GW. The microvasculature in skeletal muscle. IV. A model of the capillary network. Microvasc Res. 1986; 32(3):333–47. [PubMed: 3796306]

18. Lash JM, Bohlen HG. Functional adaptations of rat skeletal muscle arterioles to aerobic exercise training. J Appl Physiol. 1992; 72(6):2052–62. [PubMed: 1629056]
19. Takeshita S, et al. Endothelium-dependent relaxation of collateral microvessels after intramuscular gene transfer of vascular endothelial growth factor in a rat model of hindlimb ischemia. Circulation. 1998; 98(13):1261–3. [PubMed: 9751672]
20. Tanaka A, et al. Branching patterns of intramural coronary vessels determined by microangiography using synchrotron radiation. Am J Physiol. 1999; 276(6 Pt 2):H2262–7. [PubMed: 10362710]
21. Mori H, et al. Synchrotron microangiography reveals configurational changes and to-and-fro flow in intramyocardial vessels. Am J Physiol. 1999; 276(2 Pt 2):H429–37. [PubMed: 9950842]
22. Duvall CL, et al. Quantitative microcomputed tomography analysis of collateral vessel development after ischemic injury. Am J Physiol Heart Circ Physiol. 2004; 287(1):H302–10. [PubMed: 15016633]
23. Bergmann CE, et al. Arteriogenesis depends on circulating monocytes and macrophage accumulation and is severely depressed in op/op mice. J Leukoc Biol. 2006; 80(1):59–65. [PubMed: 16684892]
24. Song J, et al. Stimulation of arteriogenesis in skeletal muscle by microbubble destruction with ultrasound. Circulation. 2002; 106(12):1550–5. [PubMed: 12234963]
25. Price RJ, Skalak TC. A circumferential stress-growth rule predicts arcade arteriole formation in a network model. Microcirculation. 1995; 2(1):41–51. [PubMed: 8542539]
26. Pries AR, et al. Resistance to blood flow in microvessels in vivo. Circ Res. 1994; 75(5):904–15. [PubMed: 7923637]
27. Pries AR, Secomb TW. Control of blood vessel structure: insights from theoretical models. Am J Physiol Heart Circ Physiol. 2005; 288(3):H1010–5. [PubMed: 15706037]
28. Bearden SE, Segal SS. Neurovascular alignment in adult mouse skeletal muscles. Microcirculation. 2005; 12(2):161–7. [PubMed: 15824038]
29. O'Neill, TJt, et al. Mobilization of bone marrow-derived cells enhances the angiogenic response to hypoxia without transdifferentiation into endothelial cells. Circ Res. 2005; 97(10):1027–35. [PubMed: 16210550]
30. Hutchins GM, Miner MM, Bulkley BH. Tortuosity as an index of the age and diameter increase of coronary collateral vessels in patients after acute myocardial infarction. Am J Cardiol. 1978; 41(2):210–5. [PubMed: 623014]
31. Jackson ZS, et al. Partial off-loading of longitudinal tension induces arterial tortuosity. Arterioscler Thromb Vasc Biol. 2005; 25(5):957–62. [PubMed: 15746437]
32. Scholz D, Cai WJ, Schaper W. Arteriogenesis, a new concept of vascular adaptation in occlusive disease. Angiogenesis. 2001; 4(4):247–57. [PubMed: 12197469]
33. Silvestre JS, et al. Antiangiogenic effect of interleukin-10 in ischemia-induced angiogenesis in mice hindlimb. Circ Res. 2000; 87(6):448–52. [PubMed: 10988235]
34. Van Gieson EJ, et al. Enhanced smooth muscle cell coverage of microvessels exposed to increased hemodynamic stresses in vivo. Circ Res. 2003; 92(8):929–36. [PubMed: 12663481]
35. Scholz D, et al. Ultrastructure and molecular histology of rabbit hind-limb collateral artery growth (arteriogenesis). Virchows Arch. 2000; 436(3):257–70. [PubMed: 10782885]

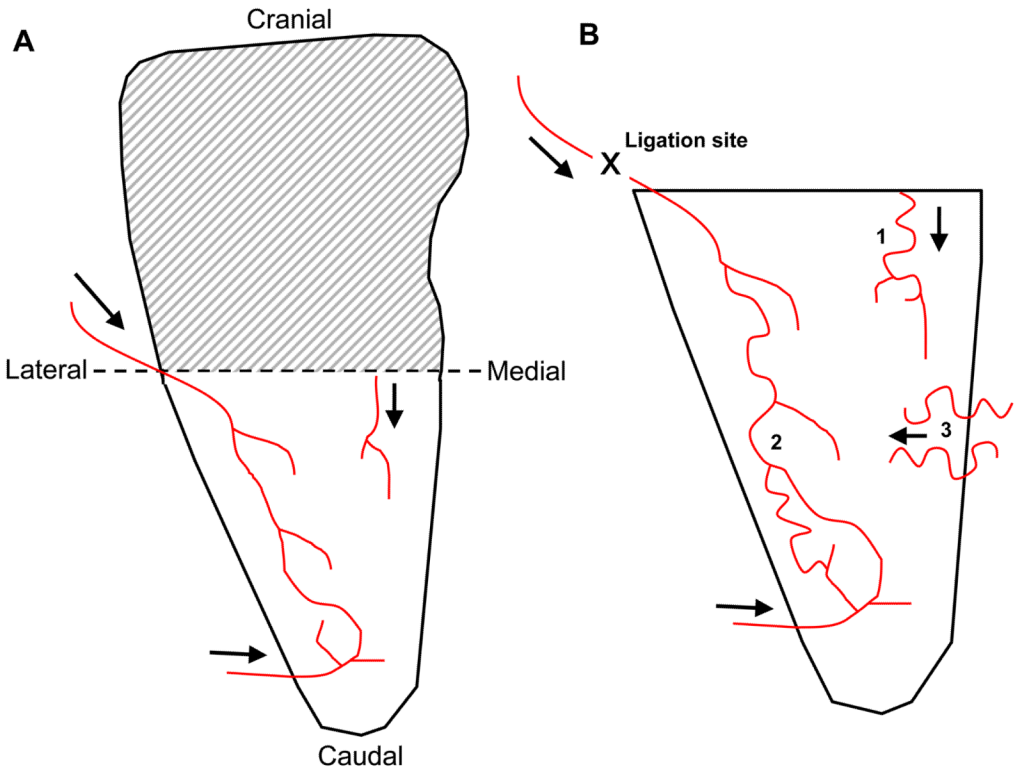

Figure 1.
Simplified cartoon representation of feeder arterioles in mouse spinotrapezius muscle with arrows showing blood flow direction. A) Microvascular remodeling occurred in the caudal-half, which was well perfused from at least three feeder arterioles. Cranial-halves of spinotrapezius muscles were not rigorously examined (shaded region). B) Enlarged view of the caudal-half of the spinotrapezius muscle showing approximate arteriole architectures and connections. Approximate placement of sutures to induce ischemic injury is marked ("X"), as are three zones where collaterogenesis was typically observed. Only collaterogenesis at zone 3 was quantified.

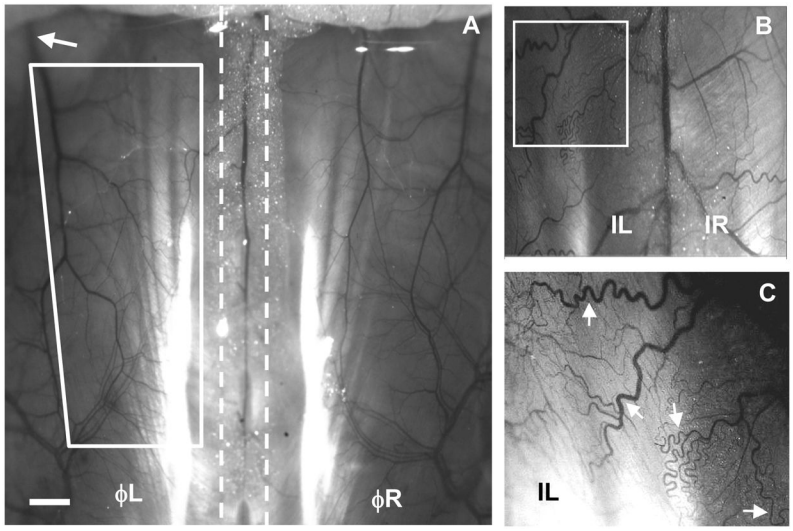

Figure 2.

Intravital microscopy images showing perfused (functional) vasculature (6.25x) in the mouse spinotrapezius muscle. A) The vasculature of the mouse spinotrapezius muscles on day 0 located to the left and right of the spine (indicated by the dashed lines). The approximate ischemic zone can be seen bounded by the four white lines. Sutures to induce the ischemic injury were placed around the feeder arteriole (approximate location upstream of white arrow) as it exited laterally from the spinotrapezius muscle. Scale bar is 1 mm. B) Intravital image digitally zoomed and enhanced. Mice that received ischemic ligations exhibited pronounced tortuosity and increased vascular branching five days post-surgery. The large vein in the center is the spinal vein, with either spinotrapezius to the left (ischemic) or right (contralateral control). Note the differing vascular architectures and pronounced vessel tortuosity on the ischemic side (white box). C) Digitally zoomed (white box) and image-enhanced view of small arterioles and venules, almost down to the capillary-level (additional digital zoom not undertaken during quantification of microvascular remodeling). A high degree of vessel tortuosity is evident (white arrows).

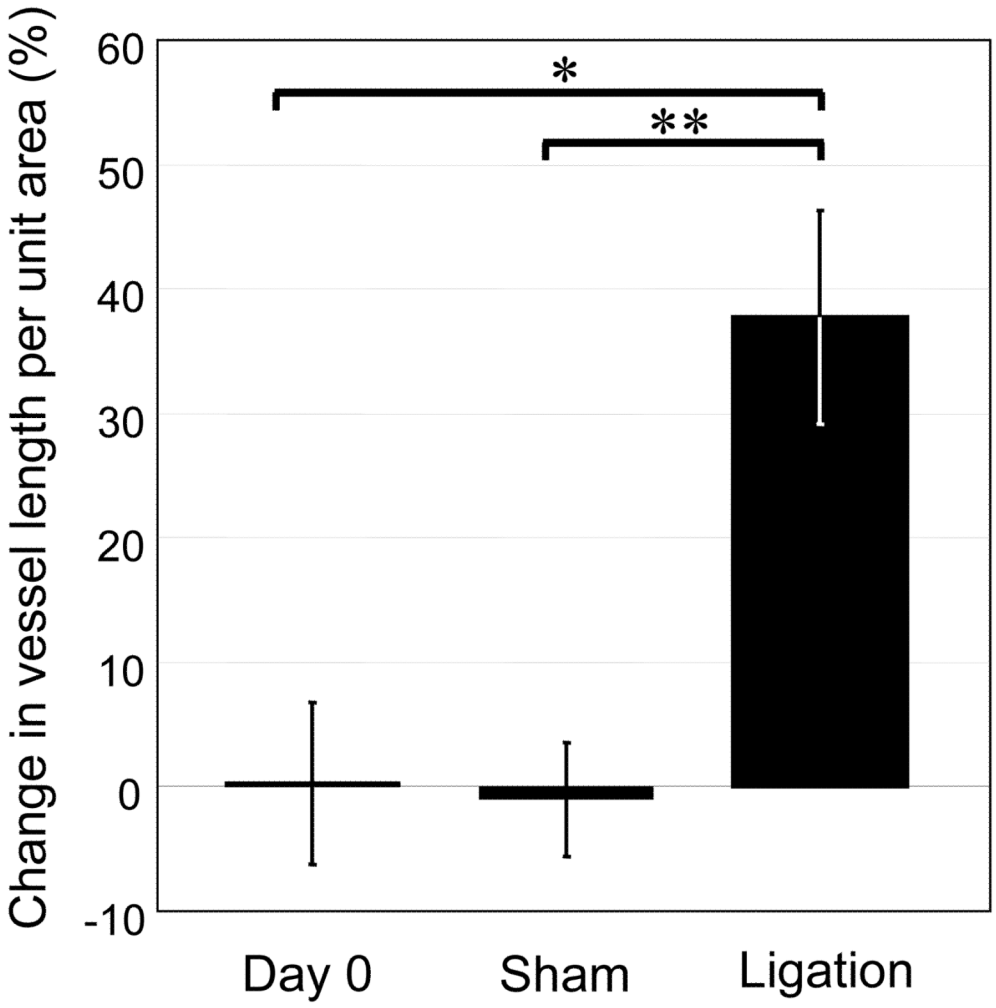

Figure 3.

Intravital microscopy. Quantification of perfused (functional) blood vessel density on day 0 (n=6) and five days after sham (n=3) or arterial ligation (n=6). Following anesthesia, exposure of the spinotrapezius muscles, and abolishment of vascular tone (maximally dilated), three to four intravital images per mouse were analyzed and average total vessel lengths per unit area were calculated. Change in length per unit area in tissues receiving an intervention (or left muscle for mice in day 0 group) are reported as a percentage of length per unit area in contralateral control (or right muscle for mice in day 0 group). Values are mean ± SD *$p \leq 0.05$.

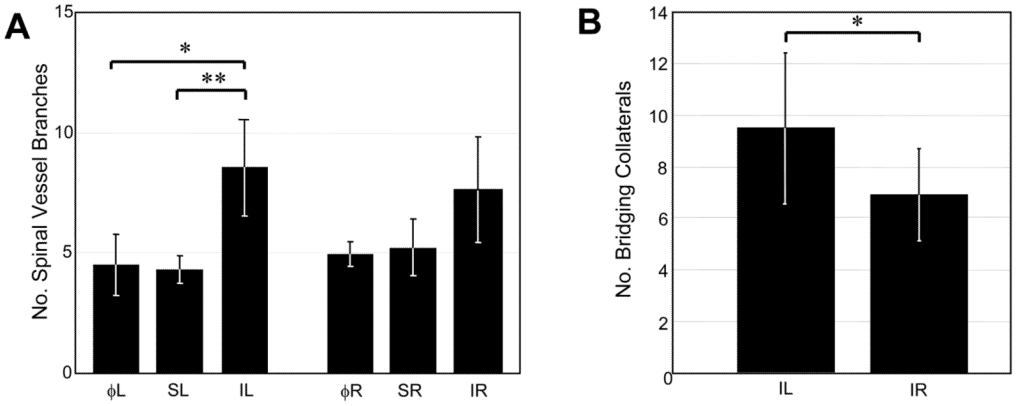

Figure 4.

Intravital microscopy. A) Quantification of spinal artery and vein branches five days post-arterial ligation (n=6), sham ligation (n=3), or at day 0 prior to any intervention (n=6). Bars correspond to muscle groups analyzed (see Methods). B) Quantification of bridging collaterals in tissues receiving ischemic ligation (IL) and their paired contralateral controls (IR) five days post-arterial ligation (n=6). Vessels were considered bridging collaterals if they crossed within 1 mm of spinal artery-vein pair, independent of origin. Values are mean ± SD *$p \leq 0.05$.

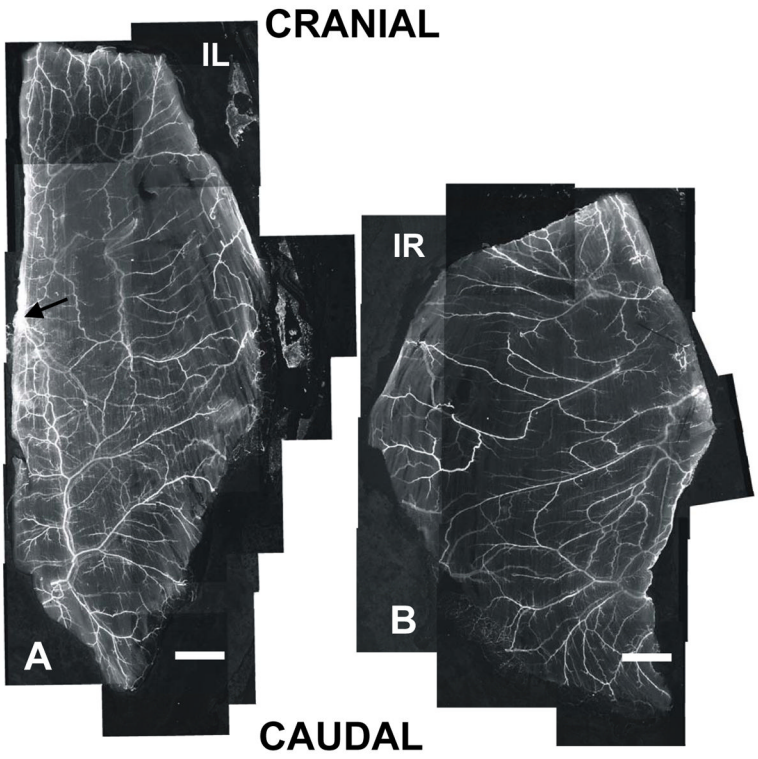

Figure 5.

Confocal microscopy. Grey-scale montages (4x) of mouse spinotrapezius muscles stained for αSMA show increased arteriolar remodeling in the ischemic muscle versus contralateral muscle. Note that the main feeding arterioles and draining venules are visible, as well as mature vessels almost down to the capillary level. A) Ischemic muscle. A region of increased αSMA coverage in the caudal-half (downstream of ligated arteriole; suture placed upstream of black arrow) is apparent, indicating a localized response. B) Contralateral control muscle. There is a decreased amount of mature vasculature and minimal vessel density variability across the length and width of the muscle. The apparent size discrepancy between muscles is due to variations in the harvesting procedure; prior to harvesting both muscles are of comparable size with similar architectures. Note that the entire 'ischemic zone' is shown here (and corresponding area in the contralateral control muscle). Scale bars are 1 mm.

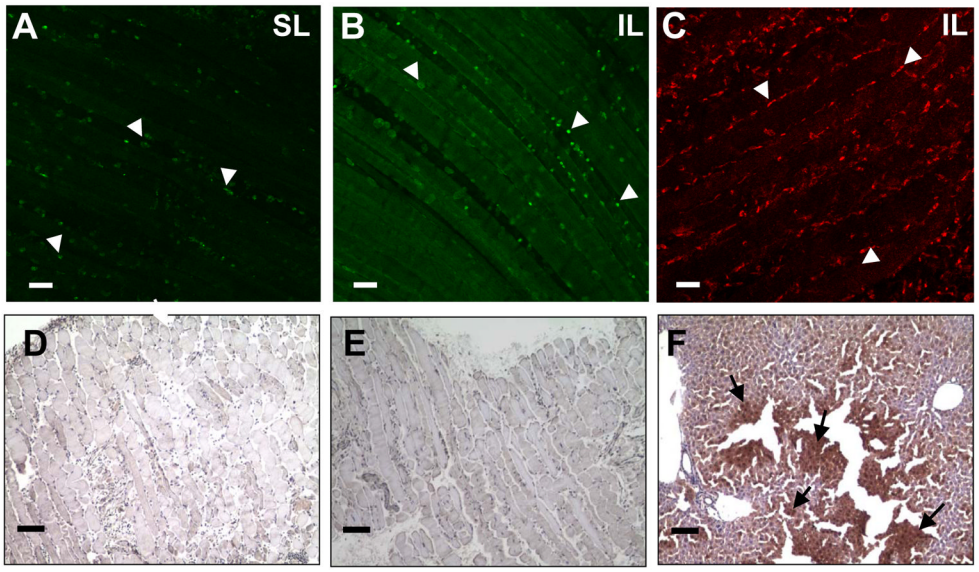

Figure 6.

Representative confocal images (20x) of tissues that underwent (A) sham ligation or (B) ischemic ligation immunolabeled for CD11b expressing cells (white arrowheads). There was a negligible presence of CD11b-expressing cells in the day 0 control tissues that received no intervention (data not shown). (C) Ischemic tissue immunolabeled with MOMA-2 antibodies showing leukocyte infiltration into injury site. Scale bars are 50 μm. Representative light microscopy images (10x) from paraffin-embedded sections of (D) sham ligation, (E) ischemic ligation, and (F) mouse liver positive-control tissues probed for the presence of hypoxic cells (Hypoxyprobe-1+ kit; Chemicon International). All skeletal muscle undergoing either ischemic or sham ligations stained negative for hypoxic cells, while the positive control, mouse liver, stained positive for hypoxic cells (black arrows). Scale bars are 100 μm.

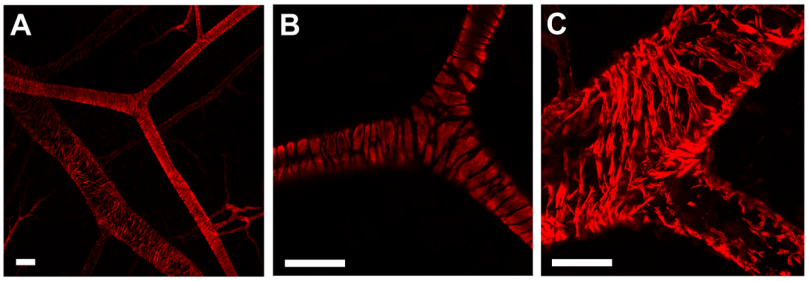

Figure 7.

Whole-mount immunolabeling of spinotrapezius muscles for αSMA using confocal microscopy. (A) Tight wrapping of VSMCs is visible on the arterioles, while a loose cobblestone morphology is evident on the venules (20x). (B) 60x image of bifurcating arteriole. (C) 60x image of venule. Note the high-level of cellular detail accessible by confocal microscopy in this model. Scale bars are 50 μm.

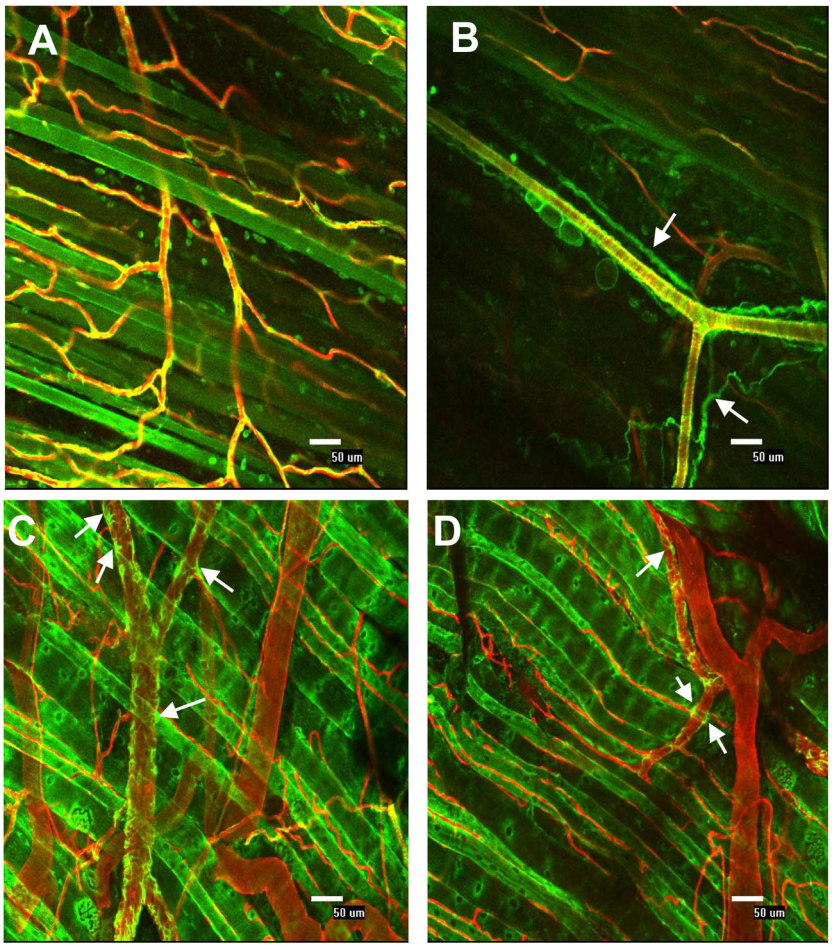

Figure 8.

Confocal microscopy (20x) and whole-mount immunolabeling of skeletal muscle microvasculature. A) Capillaries, small arterioles and venules with single cell resolution are visible. Endothelial cells labeled with BSI-lectin (red) and perivascular cells labeled with NG2 (green); Co-localization appears yellow. B) Nerve stained positive for NG2 (white arrows). C) and D) Perivascular cells stained for desmin (green) and endothelial cells stained with BSI-lectin (red). Individual perivascular cells and processes are clearly recognizable (white arrows). Muscle fibers auto-fluoresce in the green spectrum. All scale bars are 50 μm.

Table 1

Review of select *in vivo* models of arteriogenesis

Reported are the methods of inducing arteriogenesis in skeletal muscle, animal used, specific techniques employed relevant to visualization of vasculature and tissue perfusion, spatial resolution of intact vascular network (smallest quantifiable vessel diameter; NA for sectioning techniques because spatial detail is lost), smallest quantifiable vessel diameter, mode of identifying a collateral artery (CA), mode of identifying monocytes/macrophages, and qualitative observation of CA tortuosity. Included also are excerpts from the text on how arteriogenesis was defined. This table reflects the flexibility and strengths of the hindlimb ischemia models for the study of arteriogenesis. They have been instituted in numerous animals, and the severity of the injury can be varied through placement of ligation and/or excision of vessel segments. There are also numerous techniques available for the visualization of the vasculature and for the identification of collateral arteries, as well as infiltrated monocytes/macrophages. This table also highlights potential problems that arise when spatial detail is lost. For example, while arteriogenesis is typically defined as the remodeling of pre-existing arcade arterioles (collateral anastomoses), sectioning eliminates the ability to differentiate between transverse and arcade arterioles, and so this distinction on the microscale is not easily made with these models. Abbreviations are as follows—CA: collateral artery; LDPI: Laser Doppler Perfusion Imaging; MRI: Magnetic Resonance Imaging; Longland's classification: vessels must show a defined stem, midzone, and re-entry to be classified as collateral arteries.

	Arteriogenesis model	Animal	Dominant techniques	Spatial lower limit of intact network	Vessel diameter lower limit	Identification of CA	Identification of monocytes & macrophage	Tortuosity of CA
Arras et al., 1998	hindlimb; bilateral femoral artery ligation	New Zealand White rabbit	sectioning	NA	capillary	size & morphology	RAM11+ (DAKO A/S)	NA
"*in situ* proliferation of pre-existing arteriolar connections into true collateral arteries…named arteriogenesis"								
Bergmann et al., 2006	hindlimb; femoral artery ligation	op/op mouse	sectioning; angiography; microsphere perfusion	Relative and variable (~100 μm)	~15 μm arterioles	Longland's classification; αSMA+	MOMA-2+ (BMA Biomedicals); F4/80+ (Caltag labs)	corkscrew appearance
"arteriogenesis is the growth of pre-existent collateral anastomoses into functional conductance arteries"								
Brown et al., 2003	hindlimb; common iliac artery ligation	Sprague-Dawley rat	sectioning	NA	< 10 μm arterioles	αSMA+ (included all vessels)	ED1+ & ED2+ (Serotec)	NA
"…development of collateral arteries by enlargement of pre-existing connections, often referred to as arteriogenesis…."								
Couffinhal et al., 1999	hindlimb; femoral artery ligation	$ApoE^{-/us;}$mouse	sectioning; LDPI	NA	capillary	CD31+ capillary	F4/80+ (Caltag Labs)	NA
Not defined. Model of inferential collateral vessel growth via increased capillary density.								
Heil et al., 2004	hindlimb; femoral artery ligation	$CCR2^{-/-}$ mouse	LDPI; MRI; sectioning	~100 μm	CA size not explicitly defined	αSMA+	murine MAC-3 (BD Biosciences)	NA
"collateral artery growth (arteriogenesis)"								
Hoefer et al., 2004	hindlimb; femoral artery ligation	rabbit; $ICAM\text{-}1^{-/-}$ & $MAC\text{-}1^{-/-}$ mouse	angiography; sectioning	~100 μm	~15 μm arterioles	Longland's classification in angiograms; Ki-67+ (proliferating) vessels in sections	MOMA-2+ (BMA Biomedicals)	corkscrew-like collaterals

Arteriogenesis model	Animal	Dominant techniques	Spatial lower limit of intact network	Vessel diameter lower limit	Identification of CA	Identification of monocytes & macrophage	Tortuosity of CA
"In the event of arterial occlusion…a steep pressure gradient develops along the shortest path within the interconnecting network that increases blood flow velocity and hence fluid shear stress in these vessels that now assume their new function as CA. These vessels then grow to provide enhanced perfusion to the jeopardized ischemic regions. This adaptive process is termed arteriogenesis and refers to active proliferation and remodeling rather than passive dilatation."							
Hoefer et al., 2005 hindlimb; femoral artery ligation	New Zealand, White rabbit	sectioning; angiography; microsphere perfusion	~100 μm	~15 μm arterioles	Ki-67+ (proliferating) & αSMA+	CD68+ (DAKO); CD11b+ (Serotec)	not reported
"…large pressure gradient[s] over…pre-existing collateral anastomoses initiate vascular proliferation. The anastomoses with the lowest vascular resistance mature to functional arteries ensuring perfusion of the jeopardized ischemic regions. This process is referred to as arteriogenesis"							
Kinnaird et al., 2004 hindlimb; femoral artery ligation	Balb/C mouse	LDPI; sectioning	NA	capillary	Van Gieson solution; continuous internal elastic laminae (morphology)	NA	NA
"…enhanced perfusion of ischemic tissue and collateral remodeling…"							
Scholz et al., 1999 hindlimb; femoral artery ligation	New Zealand White rabbit	electron microscopy; sectioning;	NA	capillary	morphology; lower-limit of CA diameter at 100 μm	CD68+ (DAKO)	NA
"…arteriogenesis is the growth of collateral arteries from pre-existing arterioles in adults."							
Song et al., 2002 hindlimb; ultrasound-induced microbubble destruction	Sprague-Dawley rat	sectioning; microsphere perfusion	NA	capillary	αSMA+ & lectin+	NA	NA
"…formation and remodeling of arterioles, the process denoted as arteriogenesis…. This response consists of both the formation of new arterioles, which presumably occurs when preexisting capillaries acquire an SM coating, and an increase in the diameter of these newly formed and/pr preexisting arterioles into channels with larger diameters."							
Stabile et al., 2004 hindlimb; femoral artery ligation	C57/Bl6; CD8a$^{-/-}$ mouse	LDPI; sectioning	NA	capillary	Van Gieson solution; continuous internal elastic laminae + layer of muscle spindles + area > 300μm^2	CD4+ (Santa Cruz)	NA
"One of the compensatory mechanisms involved in the response to impaired blood flow secondary to atherosclerotic plaque development is the formation of collateral blood vessels. It has recently been shown that cellular components of the immune and inflammatory systems play a pivotal role in modulating collateral vessel development…[or] collaterogenesis."							
Tang et al., 2004 hindlimb; excision of femoral artery	CCR2−/− mouse	LDPI; angiography; sectioning	~200 μm	capillary	CD31+ & αSMA+	MOMA-2 (Serotec)	not reported
"…collateral artery development, or arteriogenesis…."							
Takeshita et al., 1998 hindlimb; excision of femoral artery	Wistar rat	micro-angiography; microsphere perfusion	30 μm	30 μm	morphology & location	NA	tortuous, corkscrew, as well as linear
Inconsistently defined							

Table 2

Quantification of smooth-muscle α-actin arterioles in the ischemic zone of tissues receiving ligations and in the corresponding region of contralateral control tissues. All data were collected five days post-ischemic ligation. The length density of all αSMA-positive arterioles within the ischemic zone was significantly increased over contralateral control (24% increased coverage). Conversely, the length density of αSMA-positive arcade arterioles was not significantly changed, nor were the number of arcade loops observed within ischemic zones. Abbreviations: AA, arcade arteriole.

	Ischemic (n=3)	Contralateral (n=3)
Arteriole length density, mm/mm^2	1.89 +/− 0.12*	1.53 +/− 0.09
Avg. increase, %	24.29	-
AA length density, mm/mm^2	0.61 +/− 0.21**	0.76 +/− 0.39
Avg. increase, %	−19.96	-
No. AA loops	17 +/− 5.57	17 +/− 3

* P = 0.015; Paired T-test; values are mean ± SD.